RSC Advances

PAPER

View Article Online
View Journal | View Issue

Cite this: *RSC Adv.*, 2020, **10**, 6172

Synthesis, properties and photovoltaic performance in dye-sensitized solar cells of three *meso*-diphenylbacteriochlorins bearing a dual-function electron-donor†

Subrata Chakraborty,‡ Ming-Chi Tsai,‡ Xin-De Su, Xuan-Cheng Chen, Tang-Ting Su, Che-Kai Tsao and Ching-Yao Lin *

Received 3rd December 2019
Accepted 31st January 2020

DOI: 10.1039/c9ra10113f

rsc.li/rsc-advances

Bacteriochlorins are crucial to photosynthesis in bacteria. Studies of air-stable, *meso*-substituted bacteriochlorins are rare. We herein report the synthesis, properties, and photovoltaic performance of three new air-stable, *meso*-substituted bacteriochlorins bearing a dioctylfluorenylethyne (denoted as **LS-17**), a dioctylaminophenylethynylanthrylethyne (**LS-43**), and a diarylaminoanthrylethyne (**LS-45**) as the electron-donating groups. Among these LS-bacteriochlorins, **LS-17** displays sharp UV-visible absorption bands whereas **LS-43** and **LS-45** give rise to broadened and red-shifted absorptions. Electrochemical and DFT results suggest that the first oxidation and reduction reactions of these bacteriochlorins are consistent with the formation of the cation and anion radicals, respectively. For dye-sensitized solar cell applications, photovoltaic performance of the **LS-45** cell achieves an overall efficiency of 6.04% under one-sun irradiation.

Introduction

Dye-sensitized solar cells (DSCs) have received substantial attention as an alternative and renewable power source because of the benefits of low cost, convenient fabrication procedures, and versatile choices of dyes.[1–3] Power conversion efficiencies (PCE, η) greater than 10% have been well demonstrated with the use of ruthenium complexes,[4–6] organic dyes,[7–10] and porphyrins.[11–17] It has been suggested that the photovoltaic performance of DSCs may benefit from red-shifted absorptions of the dyes.[18] Therefore, efforts have been devoted into developing dyes with near-IR absorptions. Examples have been reported to reach 900 nm while maintaining the PCE above 10%.[16,17] However, very complicated chemical structures of the dyes are required in order to achieve near-IR absorption bands.

Bacteriochlorins are planar and conjugated macrocycles with multiple absorption bands.[19] In addition to the absorption bands in near-UV (B or Soret bands) and visible region (Q_x), bacteriochlorins show very intense and characteristic absorptions in near-IR region (Q_y). Owing to this unique and important property, bacteriochlorins play key roles in the bacterial photosynthetic reaction centers, including light harvesting, energy transduction, charge separation, and electron transfer, *etc.*[20–24]

Inspired by the pioneer work of Lindsey and co-workers,[25–28] we recently reported the synthesis, fundamental properties, and photovoltaic performance of two air-stable, *meso*-substituted bacteriochlorins (denoted as **LS-01** and **LS-11**, Fig. 1).[29] To the best of our knowledge, there have been very few reports of air-stable, *meso*-aryl-substituted bacteriochlorins.[28,29] In our previous work, PCE of the DSC reached 4.67% with the use of the **LS-01** bacteriochlorin. This value outperforms that of a reference porphyrin dye with a similar structure (H2PE1, 2.06%, structure not shown). In addition, a greater PCE of 5.36% was achieved with the use of the **LS-11** dye. Importantly, we demonstrated that light harvest of DSC reached 850 nm with dyes having simple structures.

In order to improve photovoltaic performance of bacteriochlorin dyes in DSC, we prepared three new *meso*-substituted, push–pull bacteriochlorins (denoted as **LS-17**, **LS-43**, and **LS-45**, Fig. 1) and studied their fundamental properties as well as photovoltaic performance in DSC. As shown in Fig. 1, **LS-11** is included in this work as a reference dye to compare with the new dyes. **LS-11** employs a dioctylaminophenylethyne as the electron-donating group. This substituent has been used in an efficient porphyrin dye.[30] For **LS-17**, **LS-43**, and **LS-45**, they adopt electron-donating substituents from several efficient porphyrins in literature.[31–33] For **LS-17**, dioctylfluorenylethyne[31] is highly fluorescent, and the two octyl chains may improve

Department of Applied Chemistry, National Chi Nan University, No. 302 University Road, Puli, Nantou Hsien 54561, Taiwan, Republic of China. E-mail: cyl@ncnu.edu.tw; Fax: +886-49-2917956; Tel: +886-49-2910960 ext. 4152

† Electronic supplementary information (ESI) available: Details of the synthesis and characterization of the LS-bacteriochlorins, DSC fabrication and stability tests. See DOI: 10.1039/c9ra10113f

‡ These authors contributed equally.

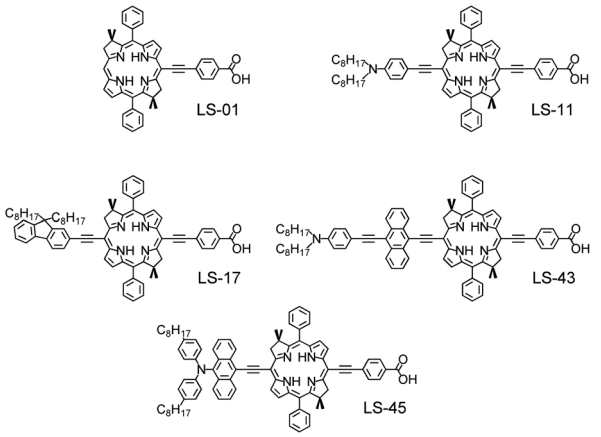

Fig. 1 Chemical structures of the LS-bacteriochlorins.

solubility of the dye in organic solvents. For **LS-43**, it employs a dioctylaminophenyl-ethynylanthrylethyne as the electron-donating group. This donor group has been shown to largely red-shift absorption bands of a porphyrin dye.[32] For **LS-45**, diarylaminoanthrylethyne was chosen to be the electron-donating group because it also broadens absorption bands of a chromophore. This dual-functioned donor has been reported to be effective for both porphyrin and organic dyes.[33,34] As will be shown below, DSC sensitized with the **LS-45** dye outperforms other dyes in this work with a PCE of 6.04%. This value is a noticeable improvement over that of reference **LS-11** dye.[29]

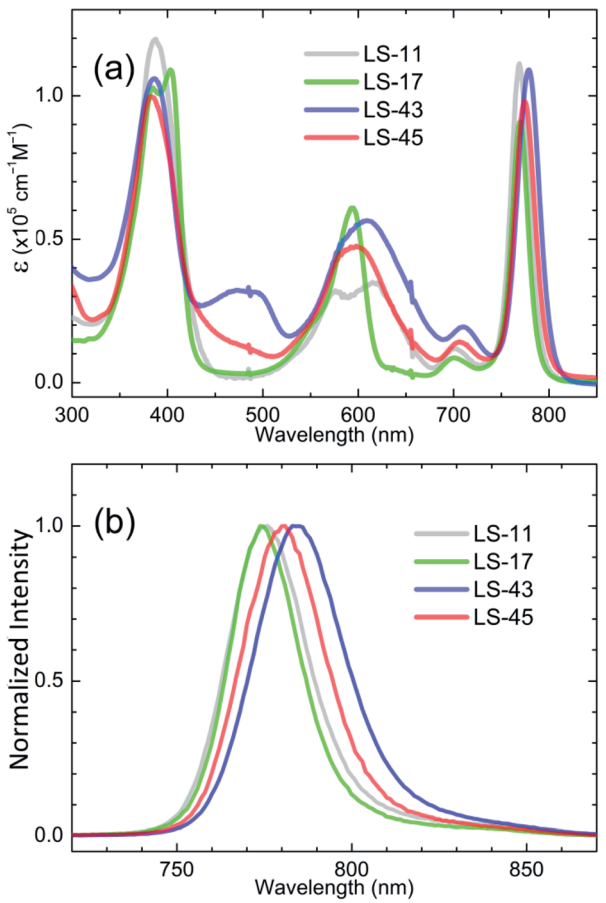

Fig. 2 (a) Absorption and (b) normalized fluorescence spectra of the LS-bacteriochlorins in THF.

Results and discussion

Synthesis

Preparation of the LS-bacteriochlorin precursor is as that described in our previous report,[29] except for the dihydrodipyrrin. Synthesis of the dihydrodipyrrin is sensitive to the composition of the $TiCl_3$ solution. Therefore, knowing the composition of the $TiCl_3$ solution is crucial to the reaction.[35] The procedure of dihydrodipyrrin synthesis is slightly adjusted in this work due to the change of $TiCl_3$ solution source (ESI†). Syntheses of the **LS-17**, **LS-43**, and **LS-45** bacteriochlorins are similar to those of related porphyrins in the literature.[29–33] Details of the syntheses and characterization data are put in the ESI.† Note that we encountered difficulties with **LS-43** during chromatographic separation and ^{13}C-NMR measurement because of the lower solubility in organic solvents. This may be related to its more extended pi-conjugation and planar chemical structure (see below).

UV-visible absorption and fluorescence emission spectra

Fig. 2 compares the (a) UV-visible spectra and (b) normalized fluorescence emission spectra of the LS-bacteriochlorins in THF. Related data are collected in Table 1. First of all, B (or Soret), Q_x, and Q_y bands of the LS bacteriochlorins are found around 390 nm, 600 nm, and 770 nm, respectively. This is consistent with the literature reports. More specifically, the B bands are observed at 388 nm for **LS-11**, 385 and 403 nm for **LS-17**, 386 nm for **LS-43**, and 383 nm for **LS-45**. In addition, **LS-17** exhibits split B bands whereas **LS-11**, **LS-43**, and **LS-45** show one broadened B bands. For the Q bands, **LS-17** gives rise to a sharper and unified Q_x band at 594 nm whereas **LS-11** (576 and 615 nm, centered at 596 nm), **LS-43** (609 nm), and **LS-45** (598 nm) exhibit broadened and split Q_x bands. In near-IR region, the Q_y bands are sharp for all LS bacteriochlorins. Although the differences are small, we observe a trend of the Q_y wavelengths as **LS-43** (779 nm) > **LS-45** (775 nm) > **LS-17** (770 nm) ~ **LS-11** (769 nm). Among the LS-bacteriochlorins, **LS-43** exhibits the most red-shifted Q_y band in the series. This phenomenon may be related to its more extended pi-conjugation and is consistent with the literature report.[32] As for the weak absorptions between the B and Q_x bands of **LS-43** and **LS-45**, these bands may be attributed to the anthracene moieties in the chemical structures. This phenomenon is consistent with that of an anthracene-modified porphyrin in literature.[36]

For fluorescence emission, the emission bands appear to be the mirror images of their corresponding Q_y bands. Also, the trend of the emission maxima is **LS-43** (784 nm) > **LS-45** (781 nm) > **LS-17** (774 nm) = **LS-11** (774 nm), consistent with the trend of the Q_y wavelengths mentioned above. As shown in

Table 1 Absorption wavelengths, fluorescence maxima, and the first macrocyclic ring redox potentials in THF/TBAP

Entry	Absorption/nm (log ε, M^{-1} cm^{-1})	Emission[b]/nm (ϕ_f[c], %)	$E_{1/2}$/V *vs.* SCE Ox(1)	Red(1)
LS-11[a]	388 (5.08), 576 (4.51), 615 (4.54), 769 (5.05)	774 (8.32)	+0.75[d]	−0.95
LS-17	385 (5.01), 403 (5.04), 594 (4.78), 770 (4.96)	774 (7.83)	+0.81	−0.92
LS-43	386 (5.02), 480 (4.51), 609 (4.76), 779 (5.04)	784 (6.07)	+0.81	−0.85
LS-45	383 (4.99), 598 (4.68), 775 (4.99)	781 (6.74)	+0.82	−0.84

[a] Taken from ref. 29. [b] Excitation wavelength/nm: **LS-11** (388), **LS-17** (403), **LS-43** (386), **LS-45** (383). [c] The quantum yields were estimated by comparing with that of 1,3,3,1′,3′,3′-hexamethyl-2,2′-indotricarbocyanine iodide (HITCI) at 688 nm. [d] Potential determined by differential pulse voltammetry due to overlapped waves.

Table 1, **LS-43** was estimated to have a lower fluorescent quantum yield than other LS-bacteriochlorins. This may be attributed to its ease of molecular aggregation. As mentioned above, we encountered difficulties during chromatographic separation and ^{13}C-NMR measurement of **LS-43** due to its lower solubility in organic solvents.

Electrochemistry, energy level and molecular orbital patterns

Fig. 3 shows cyclic voltammograms (CV) of the LS-bacteriochlorins in THF/TBAP. The first redox potentials are collected in Table 1. One reduction reaction was observed for each LS-bacteriochlorin. These reduction reactions appear as reversible redox couples at −0.95, −09.2, −0.85 and −0.84 V *vs.* SCE for **LS-11**, **LS-17**, **LS-43**, and **LS-45**, respectively. On the other hand, two oxidation waves were observed. The first oxidation potentials of **LS-11**, **LS-17**, **LS-43**, and **LS-45** were found at +0.75, +0.81, +0.81, and +0.82 V *vs.* SCE, respectively. These first reduction and oxidation potentials are consistent with those of the formation of a bacteriochlorin anion and cation radical, respectively.[29,37] Because the LS-bacteriochlorins share a common electron-withdrawing anchor (Fig. 1), differences in the redox potentials may be attributed to the various electron-donors.

Fig. 4 depicts a diagram comparing energy levels of the highest occupied molecular orbital (HOMO), the lowest unoccupied molecular orbital (LUMO) of each dye, the conduction bands (CB) of TiO_2, and the redox energy of the electrolyte. The first oxidation and reduction potentials of the LS-bacteriochlorins were used to estimate energy levels of the HOMOs and LUMOs, respectively. Importantly, LUMO levels of the dyes are considerably higher than the CB of TiO_2 whereas the HOMO levels are noticeably lower than redox energy of the electrolyte. Therefore, all LS-dyes should be capable of injecting electrons to the CB of TiO_2 upon excitation and the resulting cations can be regenerated by the electrolyte.

Fig. 5 depicts the frontier molecular orbital patterns of the LS-bacteriochlorins calculated by density-functional theory (DFT) at the B3LYP/6-31G(d,p) level.[38] Five orbitals are illustrated for each compound, from one orbital below the HOMOs to two levels above the LUMOs (or from HOMO−1 to LUMO+2). These patterns represent the pi-electron densities/probabilities of each orbital. As expected, the frontier MO patterns are consistent with the Gouterman's model with deviation.[19] For example, the HOMO−1 and HOMO resemble the so-called a_{2u} and a_{1u} orbitals, and the LUMO resembles one of the e_g orbitals. For deviation, pi-electron densities/probabilities of these MOs delocalized towards the electron-donating/withdrawing substituents, owing to the pi-conjugation through the ethynyl bridges. Also, large probabilities at the LUMO+1 levels appear at the anthryl moieties of **LS-43** and **LS-45**. They represent the anti-bonding orbitals of the anthracene, and are consistent with the literature report.[36] Importantly, the HOMO patterns concentrate

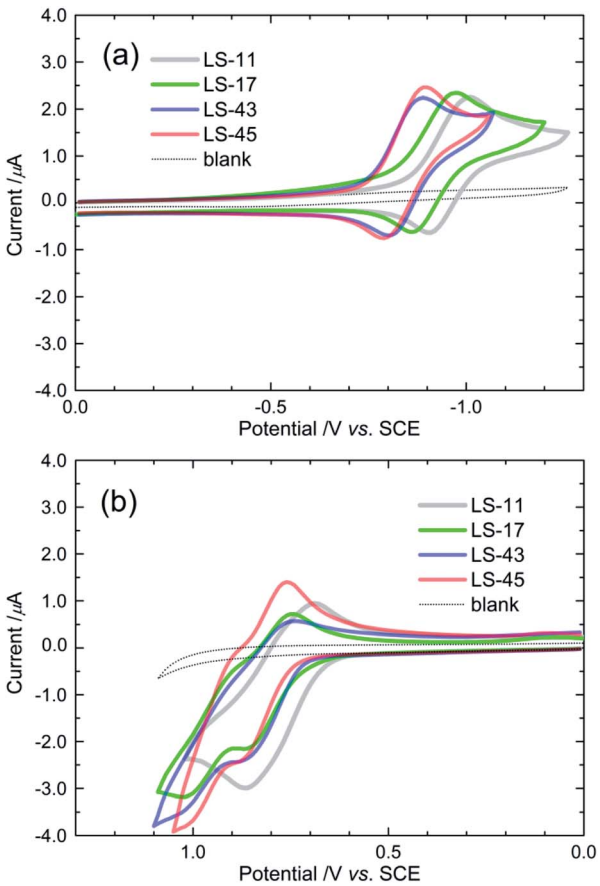

Fig. 3 Cyclic voltammograms (CVs) of the LS dyes in THF/0.1 M TBAP, showing (a) reduction and (b) oxidation reactions. CVs of the blank solution (THF/0.1 M TBAP) are shown as the dotted lines.

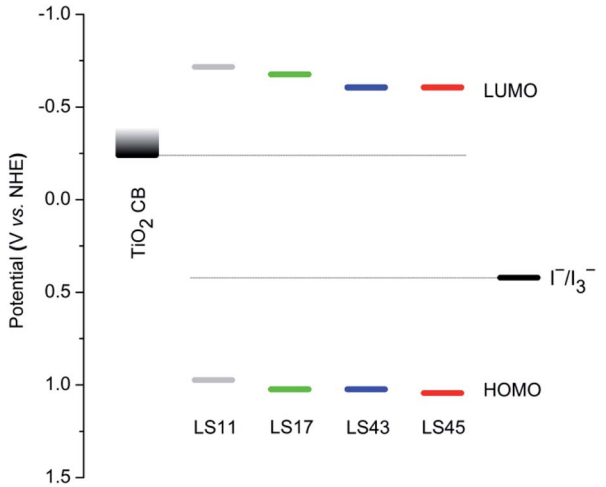

Fig. 4 Energy level diagram of TiO_2, LS dyes, and the electrolyte (I^-/I_3^-).

at the macrocyclic cores and the electron-donating substituents, whereas the LUMO, LUMO+1, or LUMO+2 patterns largely reside at the macrocycle and the electron-withdrawing substituents. This translates to a push–pull tendency of the dye, pushing the electron density from the donor groups toward the anchoring groups upon excitation. This is a welcome merit of a dye for n-type DSC application. For the optimized geometry of **LS-17** and **LS-45**, the alkyl chains are calculated to be pointing out of the bacteriochlorin planes upwards and downwards (ESI, Fig. S7†). This would increase the steric hindrance and help the dyes dissolve into organic solvents. In contrast, the alkyl chains of **LS-43** are calculated to be extending outwards into the bulk, providing little steric hinderance. This would leave the core structure susceptible to pi–pi interaction/molecular aggregation, possibly resulting in a lower solubility. This suggestion is consistent with the above-mentioned difficulties that we encountered during chromatographic separation and ^{13}C-NMR measurement of **LS-43**.

Photovoltaic properties

Fig. 5 shows (a) the current density–voltage (J–V) curves under the irradiance of 100 mW cm^{-2} simulated AM1.5 sunlight (or one-sun irradiation, solid lines) and in the dark (dotted lines) and (b) the plots of incident photon-to-electron conversion efficiency (IPCE) as a function of wavelengths of DSCs sensitized with the LS-bacteriochlorins. Related data are put in Table 2.

For PCE, we observed a trend as **LS-45** (6.04%) > **LS-11** (5.35%) > **LS-17** (5.16%) > **LS-43** (4.63%). These values are comparable with other bacteriochlorin systems reported in literature.[29,39–41] Significantly, PCE of the **LS-45** cell (6.04%) outperforms those of other devices in the series, especially that of the **LS-11** cell (5.35%). Superior performance of the **LS-45** cell may be attributed to its greater short-circuit photocurrent density (J_{sc}) and a higher open-circuit voltage (V_{oc}). For J_{sc}, we observed a trend as **LS-45** (17.43 mA cm^{-2}) > **LS-11** (16.13 mA cm^{-2}) > **LS-17** (14.90 mA cm^{-2}) > **LS-43** (14.67 mA cm^{-2}). The greater J_{sc} value of the **LS-45** cell may be related to its broadened and intense IPCE spectrum with no apparent gaps/dips.

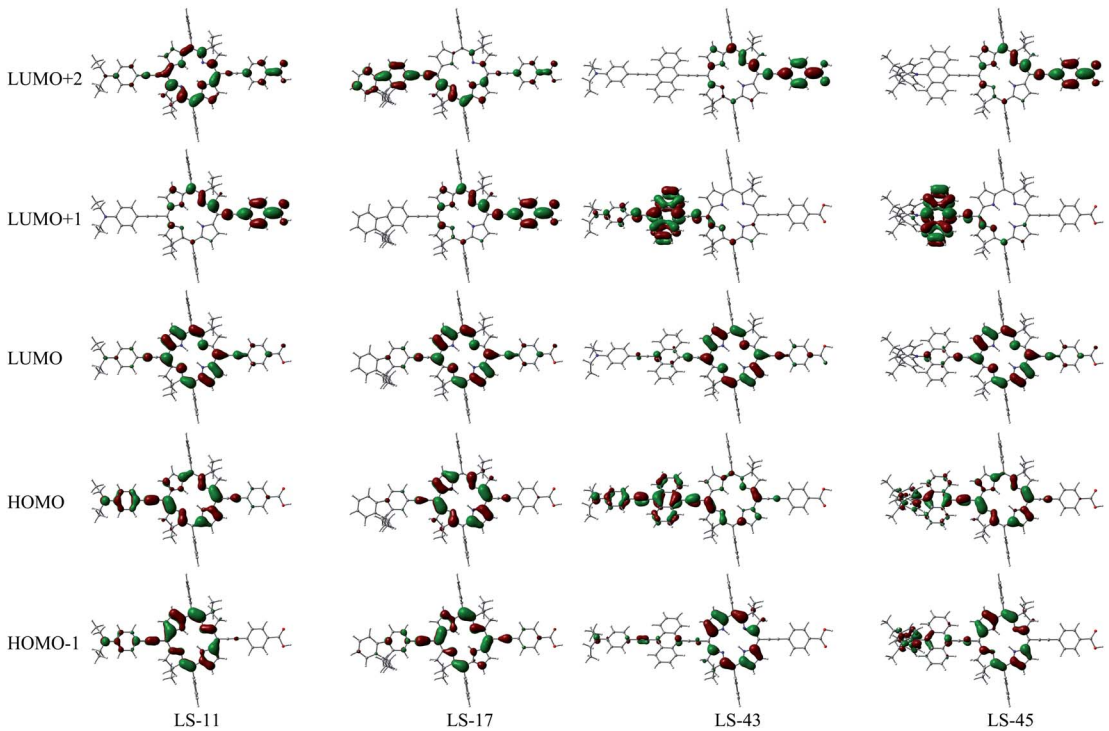

Fig. 5 Frontier molecular orbitals of the LS dyes, calculated by DFT at B3LYP/6-31(d,p). For clarity, the octyl chains were represented by ethyl groups in calculations.

Table 2 Parameters of the LS-sensitized solar cells[a]

Dye	J_{sc}^{IPCE}[b] (mA cm^{-2})	J_{sc} (mA cm^{-2})	V_{oc} (V)	FF	η (%)
LS-11	14.90	16.13 ± 0.20	0.52 ± 0.00	0.64 ± 0.01	5.35 ± 0.03
LS-17	13.83	14.90 ± 0.51	0.54 ± 0.00	0.64 ± 0.00	5.16 ± 0.15
LS-43	13.86	14.67 ± 0.23	0.52 ± 0.00	0.61 ± 0.00	4.63 ± 0.09
LS-45	15.26	17.43 ± 0.42	0.54 ± 0.01	0.64 ± 0.01	6.04 ± 0.05

[a] The photovoltaic parameters were obtained under simulated AM-1.5 G illumination (power density 100 mW cm^{-2}). The active area was 0.25 cm^2 with a black mask of area 0.16 cm^2 for each cell. These parameters are averaged values of 5, 4, 4, and 5 cells for **LS-11**, **LS-17**, **LS-43**, and **LS-45**, respectively. [b] To compare with the J_{sc} obtained from the *J–V* measurements, J_{sc}^{IPCE} is derived *via* wavelength integration of the IPCE spectra.

Between **LS-45** and **LS-11**, Fig. 6b shows that IPCE of the **LS-45** cell outperforms that of the **LS-11** device around 480 nm and beyond 800 nm. As a result, the **LS-45** cell exhibiting a greater integrated J_{sc} value (J_{sc}^{IPCE}, Table 2). For V_{oc}, V_{oc} of the **LS-45** cell is higher than that of the **LS-11** device. This is consistent with its later occurrence of the dark current of the **LS-45** cell (Fig. 6a, red dotted line). Although the overall efficiency of the **LS-43** cell is the poorest in the series, it does give rise to the most red-shifted IPCE spectrum, arriving at 920 nm.

Dye-loadings on the photo-anodes may also affect photovoltaic performance of DSCs. Therefore, dye-loadings of the LS-dyes on the photo-anodes were estimated by soaking the fully loaded photo-anodes in 0.01 M of tetrabutylammonium hydroxide (TBAOH) in THF. The results show that 110, 230, 280, and 180 nmol cm^{-2} of **LS-11**, **LS-17**, **LS-43**, and **LS-45** molecules were de-sorbed from the TiO_2 anodes, respectively. Note that the **LS-43** photo-anode carries the most dye molecules in the series. Yet, the **LS-43** cell gives rise to the poorest photovoltaic performance. This may be caused by dye aggregation of **LS-43** on the photo-anode. This suggestion is consistent with the above-mentioned difficulties during chromatographic separation and ^{13}C-NMR measurement of **LS-43**.

Because **LS-45** outperforms other dyes in this work, we therefore focus on comparing only **LS-45** with **LS-11** in the following experiments. Electrochemical impedance spectroscopy (EIS), intensity-modulated photovoltage spectroscopy (IMVS) and intensity-modulated photocurrent spectroscopy (IMPS) analyses were carried out in order to better understand the superior performance of the **LS-45** cell over that of the **LS-11** cell. Fig. 7 compares Nyquist plots of the **LS-11** and **LS-45** cells (a) under one-sun irradiation and (b) in the dark. Plots of (c) chemical capacitance (C_μ) and (d) recombination resistance (R_{rec}) *vs.* applied voltages were also obtained based on the equivalent circuit model (inset in Fig. 7d). As shown in Fig. 7a, EIS responses from both cells are similar under one-sun irradiation. For Fig. 7b, the difference is more apparent in the dark. Three semicircles are expected in this figure. One small semicircle in the lower frequency region (from 0.1 Hz to 2 Hz) is associated with ion diffusion in the electrolyte. One larger

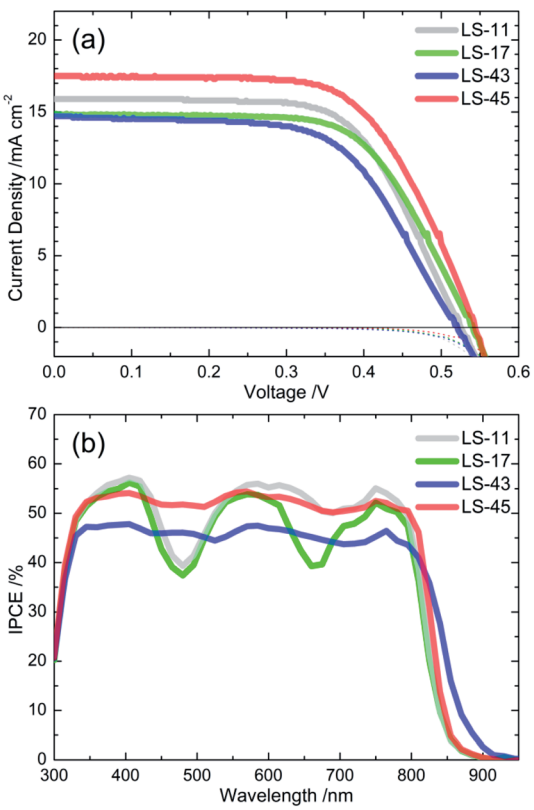

Fig. 6 (a) *J–V* curves and (b) IPCE spectra of LS dye-sensitized solar cells. Overall efficiencies of these specific cells are 5.36% for **LS-11**, 5.15% for **LS-17**, 4.63% for **LS-43**, and 6.02% for **LS-45**.

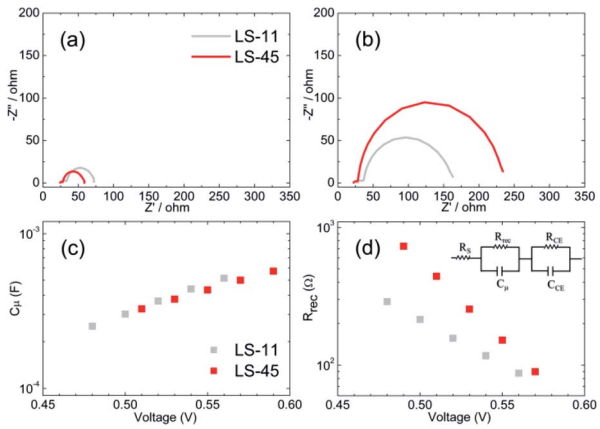

Fig. 7 Nyquist plots of the **LS-11** and **LS-45** cells (a) under one-sun irradiation and (b) in the dark. Based on the equivalent circuit model (inset in (d)), (c) chemical capacitance (C_μ) and (d) recombination resistance (R_{rec}) *vs.* applied voltages were also obtained.

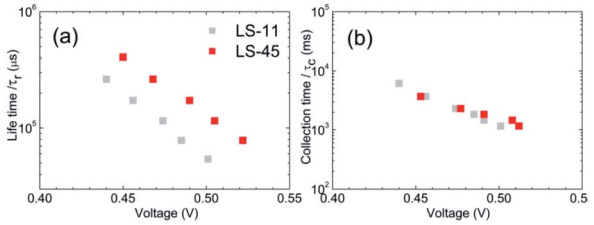

Fig. 8 Plots of (a) life time (τ_r), and (b) collection time *vs.* applied voltages for **LS-11** and **LS-45** cells.

semicircle in the middle frequency region (from 2 Hz to 1 kHz) is related to the charge-recombination at the TiO_2/dye/electrolyte interface. And another small semicircle at the higher frequency region (>1 kHz) is corresponding with the charge-transfer processes at the Pt/electrolyte interface.[42] Occasionally, as in the case of Fig. 7b and a large middle-frequency semicircle may obscure the smaller semicircles. A larger resistance in the middle frequency region suggests a lower tendency of charge recombination, contributing to a higher V_{oc} and a lower dark current. This is consistent with what we observed for the **LS-45** and **LS-11** cells in Fig. 6a and Table 2. In Fig. 7c, the fitted C_μ values are similar for both cells, suggesting that chemical capacitance may not be a major factor affecting the photovoltaic performance. In Fig. 7d, one observes a greater R_{rec} value of the **LS-45** cell than that of the **LS-11** cell at a fixed applied voltage. This is consistent with the **LS-45** cell having a greater V_{oc}. For IMVS and IMPS, Fig. 8 compares (a) lifetime (τ_r), and (b) collection time (τ_c) against applied voltages. The plot in Fig. 8a shows a trend of τ_r as **LS-45** > **LS-11** at a fixed applied voltage. A greater τ_r value of the **LS-45** cell is consistent with its greater recombination resistance (R_{rec}, Fig. 7d), contributing to a higher V_{oc}. For collection time, Fig. 8b shows little difference between the **LS-45** and **LS-11** cells. Again, this suggests that collection time may not be a major factor affecting the overall efficiency.

Conclusions

In this work, we report the synthesis, fundamental properties, and photovoltaic performance in DSC of three new *meso*-diphenylbacteriochlorins. The **LS-17**, **LS-43**, and **LS-45** bacteriochlorins bear a dioctylfluorenylethyne, a dioctylaminophenylethynylanthrylethyne, and a diarylaminoanthrylethyne as the electron-donating groups, respectively. By using the **LS-11** dye from our previous work as a reference, **LS-17** shows sharp UV-visible absorption bands whereas **LS-43** and **LS-45** exhibit broadened and red-shifted absorptions. Electrochemical results and DFT-calculated MO patterns suggest that the first oxidation and reduction reactions are consistent with the formation of bacteriochlorin cation and anion radicals, respectively. The energy level diagram suggests that the new bacteriochlorins are suitable for DSC application. The *J*–*V* and IPCE studies show that **LS-45** outperforms others in the series with a PCE of 6.04%. Superior PCE of **LS-45** may be attributed to the greater J_{sc} and V_{oc} values. A greater J_{sc} is consistent with a broadened and red-shifted IPCE spectrum with no apparent dips. EIS, IMPS, and IMVS measurements suggest that the higher V_{oc} of the **LS-45** cell may be attributed to a greater charge recombination resistance. As to remedy the possible issue of molecular aggregation, synthesis of more soluble version of the LS-bacteriochlorins are underway.

Conflicts of interest

There are no conflicts to declare.

Acknowledgements

We are grateful for the support of the Ministry of Science and Technology, Taiwan (MOST 105-2119-M-260-003-MY3, MOST 106-2119-M-260-001, and MOST 106-2811-M-260-001). We very much thank Prof. J. S. Lindsey for the useful discussions.

Notes and references

1 M. Grätzel, *Nature*, 2001, **414**, 338–344.
2 B. O'Regan and M. Grätzel, *Nature*, 1991, **353**, 737–740.
3 M. Grätzel, *Inorg. Chem.*, 2005, **44**, 6841–6851.
4 M. K. Nazeeruddin, F. De Angelis, S. Fantacci, A. Selloni, G. Viscardi, P. Liska, S. Ito, B. Takeru and M. Grätzel, *J. Am. Chem. Soc.*, 2005, **127**, 16835–16847.
5 F. Gao, Y. Wang, D. Shi, J. Zhang, M. Wang, X. Jing, R. Humphry-Baker, P. Wang, S. M. Zakeeruddin and M. Grätzel, *J. Am. Chem. Soc.*, 2008, **130**, 10720–10728.
6 C.-Y. Chen, M. Wang, J.-Y. Li, N. Pootrakulchote, L. Alibabaei, C.-H. Ngocle, J.-D. Decoppet, J.-H. Tsai, C. Grätzel, C.-G. Wu, S. M. Zakeeruddin and M. Grätzel, *ACS Nano*, 2009, **3**, 3103–3109.
7 Y. Cao, Y. Liu, S. M. Zakeeruddin, A. Hagfeldt and M. Grätzel, *Joule*, 2018, **2**, 1108–1117.
8 K. Kakiage, Y. Aoyama, T. Yano, K. Oya, J.-I. Fujisawa and M. Hanaya, *Chem. Commun.*, 2015, **51**, 15894–15897.
9 Z. Yao, H. Wu, Y. Li, J. Wang, J. Zhang, M. Zhang, Y. Guo and P. Wang, *Energy Environ. Sci.*, 2015, **8**, 3192–3197.
10 Y. Ezhumalai, B. Lee, M.-S. Fan, B. Harutyunyan, K. Prabakaran, C.-P. Lee, S. H. Chang, J.-S. Ni, S. Vegiraju, P. Priyanka, Y.-W. Wu, C.-W. Liu, S. Yau, J. T. Lin, C.-G. Wu, M. J. Bedzyk, R. P. H. Chang, M.-C. Chen, K.-C. Ho and T. J. Marks, *J. Mater. Chem. A*, 2017, **5**, 12310–12321.
11 M. Urbani, M. Grätzel, M. K. Nazeeruddin and T. Torres, *Chem. Rev.*, 2014, **114**, 12330–12396.
12 T. Higashinoa and H. Imahori, *Dalton Trans.*, 2015, **44**, 448–463.
13 L.-L. Li and E. W.-G. Diau, *Chem. Soc. Rev.*, 2013, **42**, 291–304.
14 Y. K. Eom, S. H. Kang, I. T. Choi, Y. Yoo, J. Kim and H. K. Kim, *J. Mater. Chem. A*, 2017, **5**, 2297–2308.
15 S. Mathew, A. Yella, P. Gao, R. Humphry-Baker, B. F. E. Curchod, N. Ashari-Astani, I. Tavernelli, U. Rothlisberger, M. K. Nazeeruddin and M. Grätzel, *Nat. Chem.*, 2014, **6**, 242–247.

16 H.-P. Wu, Z.-W. Ou, T.-Y. Pan, C.-M. Lan, W.-K. Huang, H.-W. Lee, N. M. Reddy, C.-T. Chen, W.-S. Chao, C.-Y. Yeh and E. W.-G. Diau, *Energy Environ. Sci.*, 2012, **5**, 9843–9848.
17 J.-W. Shiu, Y.-C. Chang, C.-Y. Chan, H.-P. Wu, H.-Y. Hsu, C.-L. Wang, C.-Y. Lin and E. W.-G. Diau, *J. Mater. Chem. A*, 2015, **3**, 1417–1420.
18 T. W. Hamann, R. A. Jensen, A. B. F. Martinson, H. V. Ryswykac and J. T. Hupp, *Energy Environ. Sci.*, 2008, **1**, 66–78.
19 M. Gouterman, *J. Mol. Spectrosc.*, 1961, **6**, 138–163.
20 J. Deisenhofer, O. Epp, K. Miki, R. Huber and H. Michel, *Nature*, 1985, **318**, 618–624.
21 J. P. Allen, G. Feher, T. O. Yeates, H. Komiya and D. C. Rees, *Proc. Natl. Acad. Sci. U.S.A.*, 1987, **84**, 6162–6166.
22 G. McDermott, S. M. Prince, A. A. Freer, A. M. Hawthornthwaite-Lawless, M. Z. Papiz, R. J. Cogdell and N. W. Isaacs, *Nature*, 1995, **374**, 517–521.
23 H. Scheer, *Chlorophylls*, CRC, Boca Raton, FL, U.S.A., 1991.
24 J. Barber and B. Andersson, *Nature*, 1994, **370**, 31–34.
25 H.-J. Kim and J. S. Lindsey, *J. Org. Chem.*, 2005, **70**, 5475–5486.
26 D. Fan, M. Taniguchi and J. S. Lindsey, *J. Org. Chem.*, 2007, **72**, 5350–5357.
27 J. R. Stromberg, A. Marton, H. L. Kee, C. Kirmaier, J. R. Diers, C. Muthiah, M. Taniguchi, J. S. Lindsey, D. F. Bocian, G. J. Meyer and D. Holten, *J. Phys. Chem. C*, 2007, **111**, 15464–15478.
28 Y. Liu and J. S. Lindsey, *J. Org. Chem.*, 2016, **81**, 11882–11897.
29 S. Chakraborty, H.-C. You, C.-K. Huang, B.-Z. Lin, C.-L. Wang, M.-C. Tsai, C.-L. Liu and C.-Y. Lin, *J. Phys. Chem. C*, 2017, **121**, 7081–7087. It has been brought to our attention that the weight of the yellow product on page S14 in the SI† of of this report was mistyped. It should be 1.084 g, not 158 mg. Nonetheless, the yield was correctly reported.
30 C.-L. Wang, C.-M. Lan, S.-H. Hong, Y.-F. Wang, T.-Y. Pan, C.-W. Chang, H.-H. Kuo, M.-Y. Kuo, E. W.-G. Diau and C.-Y. Lin, *Energy Environ. Sci.*, 2012, **5**, 6933–6940.
31 C.-H. Wu, S.-H. Hong, H.-H. Kuo, Y.-Y. Chu, E. W.-G. Diau and C.-Y. Lin, *Chem. Commun.*, 2012, **48**, 4329–4331.
32 C.-L. Wang, J.-Y. Hu, C.-H. Wu, H.-H. Kuo, Y.-C. Chang, Z.-J. Lan, H.-P. Wu, E. W.-G. Diau and C.-Y. Lin, *Energy Environ. Sci.*, 2014, **7**, 1392–1396.
33 C.-L. Wang, M. Zhang, Y.-H. Hsiao, C.-K. Tseng, C.-L. Liu, M. Xu, P. Wang and C.-Y. Lin, *Energy Environ. Sci.*, 2016, **9**, 200–206.
34 Y. Wang, B. Chen, W. Wu, X. Li, W. Zhu, H. Tian and Y. Xie, *Angew. Chem., Int. Ed.*, 2014, **53**, 10779–10783.
35 C.-Y. Chen, D. F. Bocian and J. S. Lindsey, *J. Org. Chem.*, 2014, **79**, 1001–1016.
36 C.-Y. Lin, Y.-C. Wang, S.-J. Hsu, C.-F. Lo and E. W.-G. Diau, *J. Phys. Chem. C*, 2010, **114**, 687–693.
37 C.-Y. Lin, M. E. Blackwood Jr, R. Kumble, S. Hu and T. G. Spiro, *J. Phys. Chem. B*, 1997, **101**, 2372–2380.
38 M. J. Frisch, *et. al.*, *Gaussian 03, Revision D.01*, Gaussian, Inc., Pittsburgh PA, 2003.
39 X.-F. Wang, O. Kitao, H. Zhou, H. Tamiaki and S.-I. Sasaki, *J. Phys. Chem. C*, 2009, **113**, 7954–7961.
40 X.-F. Wang, Y. Koyama, H. Nagae, Y. Wada, S.-I. Sasaki and H. Tamiaki, *J. Phys. Chem. C*, 2008, **112**, 4418–4426.
41 T. Higashino, Y. Tsuji, Y. Fujimori, K. Sugiura, S. Ito and H. Imahori, *Chem. Lett.*, 2015, **44**, 1395–1397.
42 L.-L. Li, Y.-C. Chang, H.-P. Wu and E. W.-G. Diau, *Int. Rev. Phys. Chem.*, 2012, **31**, 420–467.

